Eur. Phys. J. C (2015) 75:438
DOI 10.1140/epjc/s10052-015-3662-8

THE EUROPEAN PHYSICAL JOURNAL C

Regular Article - Theoretical Physics

Diffractive dissociation in high energy pp collisions in additive quark model

Yu. M. Shabelski[a], **A. G. Shuvaev**[b]

Petersburg Nuclear Physics Institute, Kurchatov National Research Center, Gatchina, Saint Petersburg 188300, Russia

Received: 21 April 2015 / Accepted: 6 September 2015 / Published online: 21 September 2015

Abstract High energy (CERN SPS and LHC) pp ($p\bar{p}$) scattering is treated in the framework of the Additive Quark Model together with Pomeron exchange theory. Reasonable agreement with experimental data is achieved both for the elastic scattering and for the diffractive dissociation with natural parameters for the strong matter distribution inside proton.

1 Introduction

Regge theory provides a useful tool for the phenomenological description of high energy hadron collisions [1–4]. The quantitative predictions of Regge calculus are essentially dependent on the assumed coupling of participating hadrons to the Pomeron. In our previous paper [5] we described elastic pp ($p\bar{p}$) scattering including the recent LHC data in terms of a simple Regge exchange approach in the framework of the Additive Quark Model (AQM) [6,7]. In the present paper we extend our description to the processes of single and double diffractive dissociation.

In AQM the baryon is treated as a system of three spatially separated compact objects – the constituent quarks. Each constituent quark is colored and has an internal quark–gluon structure and a finite radius that is much less than the radius of the proton, $r_q^2 \ll r_p^2$. This picture is in good agreement both with $SU(3)$ symmetry of the strong interaction and the quark–gluon structure of the proton [8,9]. The constituent quarks play the roles of incident particles in terms of which pp (or πp) scattering is described in AQM [6].

The transverse range of the interaction increases with the energy [10], while the AQM approach is reliable until $r_q^2 \ll r_p^2$. When $r_q^2 \simeq r_p^2$ the AQM relations between the cross sections are modified by Gribov universality [10] (i.e. the ratio $\sigma_{pp}^{\rm tot}/\sigma_{\pi p}^{\rm tot} = 3/2$ valid for not very high energies transforms with the energy growth into $\sigma_{pp}^{\rm tot}/\sigma_{\pi p}^{\rm tot} \simeq 1$). In the present calculations we assume that the LHC energies are not high enough for Gribov universality.

To make the main ingredients and notations of our approach clearer we start from the elastic scattering in Sect. 2. The formalism used to describe single and double diffractive dissociation is presented in Sect. 3, while the obtained numerical results are compared with the experimental data in Sect. 4.

2 Elastic scattering amplitude in AQM

Elastic amplitudes for large energy $s = (p_1 + p_2)^2$ and small momentum transfer t are dominated by Pomeron exchange. We neglect the small difference in pp and $p\bar{p}$ scattering coming from the exchange of negative signature Reggeons, Odderon (see e.g. [11] and references therein), ω-Reggeon etc., since their contribution is suppressed by s.

The single t-channel exchange results into the amplitude of constituent quarks scattering

$$M_{qq}^{(1)}(s,t) = \gamma_{qq}(t) \cdot \left(\frac{s}{s_0}\right)^{\alpha_P(t)-1} \cdot \eta_P(t), \qquad (1)$$

where $\alpha_P(t) = \alpha_P(0) + \alpha'_P \cdot t$ is the Pomeron trajectory specified by the intercept, $\alpha_P(0)$, and slope, α'_P, values. The Pomeron signature factor,

$$\eta_P(t) = i - \tan^{-1}\left(\frac{\pi\alpha_P(t)}{2}\right),$$

determines the complex structure of the amplitude. The factor $\gamma_{qq}(t) = g_1(t) \cdot g_2(t)$ has the meaning of the Pomeron coupling to the beam and target particles, the functions $g_{1,2}(t)$ being the vertices of the constituent quark–Pomeron interaction (filled circles in Fig. 1).

Due to factorization of the longitudinal and transverse degrees of freedom the longitudinal momenta are integrated

[a] e-mail: shabelsk@thd.pnpi.spb.ru

[b] e-mail: shuvaev@thd.pnpi.spb.ru

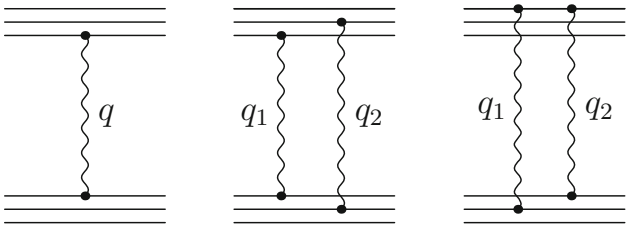

Fig. 1 The AQM diagrams for pp elastic scattering. The *straight lines* stand for quarks, the *waved lines* denote Pomerons, Q is the momentum transferred, $t = -Q^2$. **a** The one of the single Pomeron diagrams, **b** and **c** represent double Pomeron exchange with two Pomerons coupled to a different quark (**b**) and to the same quarks (**c**), $q_1 + q_2 = Q$

over separately in the high energy limit. After this the transverse part of the quark distribution is actually relevant only. It is described by the wave function $\psi(k_1, k_2, k_3)$, where the k_i are the quark transverse momenta, normalized as

$$\int \mathrm{d}K\, |\psi(k_1, k_2, k_3)|^2 \,=\, 1, \tag{2}$$

and a shorthand notation is used,

$$\mathrm{d}K \,\equiv\, \mathrm{d}^2k_1\mathrm{d}^2k_2\mathrm{d}^2k_3\,\delta^{(2)}(k_1 + k_2 + k_3).$$

The elastic pp (or $p\bar{p}$, here we do not distinguish between them) scattering amplitude is basically expressed in terms of the wave function as

$$M_{pp}(s,t) = \int \mathrm{d}K\,\mathrm{d}K'\psi^*(k_i' + Q_i')\,\psi^*(k_i + Q_i) \times V(Q, Q')\,\psi(k_i')\,\psi(k_i). \tag{3}$$

In this formula $\psi(k_i) \equiv \psi(k_1, k_2, k_3)$ is the initial proton wave function, $\psi(k_i+Q_i) \equiv \psi(k_1+Q_1, k_2+Q_2, k_3+Q_3)$ is the wave function of the scattered proton, and the interaction vertex $V(Q, Q') \equiv V(Q_1, Q_2, Q_3, Q_1', Q_2', Q_3')$ stands for the multipomeron exchange. Q_k and Q_l' are the momenta transferred to the target quark k or beam quark l by the Pomerons attached to them, Q is the total momentum transferred in the scattering, $Q^2 = -t$.

The scattering amplitude is presented in AQM as a sum over the terms with a given number of Pomerons,

$$M_{pp}(s,t) \,=\, \sum_n M_{pp}^{(n)}(s,t), \tag{4}$$

where the amplitudes $M_{pp}^{(n)}$ collect all diagrams comprising various connections of the beam and target quark lines with n Pomerons.

Similar to Glauber theory [12,13] one has to rule out the multiple interactions between the same quark pair. AQM permits the Pomeron to connect any two quark lines only once. It crucially decreases the combinatorics, leaving the diagrams with no more than $n = 9$ effective Pomerons. Several AQM diagrams are shown in Fig. 1.

In what follows we assume the Pomeron trajectory in the simplest form,

$$\left(\frac{s}{s_0}\right)^{\alpha_P(t)-1} \,=\, \mathrm{e}^{\Delta\cdot\xi}\mathrm{e}^{-r_q^2\,q^2}, \quad \xi \equiv \ln\frac{s}{s_0}, \quad r_q^2 \equiv \alpha'\cdot\xi.$$

The value r_q^2 defines the radius of the quark–quark interaction, while $S_0 = (9\ \mathrm{GeV})^2$ has the meaning of the typical energy scale in Regge theory.

In the first order there are nine equal quark–quark contributions due to one Pomeron exchange between qq pairs. The amplitude (3) reduces to a single term with $Q_1 = Q_1' = Q$, $Q_{2,3} = Q_{2,3}' = 0$,

$$M_{pp}^{(1)} \,=\, 9(\gamma_{qq}\eta_P(t)\mathrm{e}^{\Delta\cdot\xi})\,\mathrm{e}^{-r_q^2\,Q^2}F_P(Q,0,0)^2, \tag{5}$$

expressed through the overlap function

$$F_P(Q_1, Q_2, Q_3) \,=\, \int \mathrm{d}K\,\psi^*(k_1, k_2, k_3) \times\psi(k_1 + Q_1, k_2 + Q_2, k_3 + Q_3). \tag{6}$$

The function $F_P(Q, 0, 0)$ plays the role of the proton form factor for the strong interaction in AQM.

An example of the second order diagrams is shown in Fig. 1b, c. Denoting by $q_{1,2}$ the transverse momenta carried by the Pomerons, we have for diagram b $Q_1 = Q_3' = 0$, $Q_2 = Q_2' = q_2$, $Q_3 = Q_1' = q_1$ and for diagram c $Q_1 = q_1 + q_2$, $Q_2 = Q_3 = 0$, $Q_2' = q_1$, $Q_3' = 0$.

Generally, the higher orders elastic terms are expressed through the functions (6) integrated over the Pomerons' momenta,

$$M^{(n)}(s,t) \,=\, i^{n-1}(\gamma_{qq}\eta_P(t_n)\mathrm{e}^{\Delta\cdot\xi})^n \times\int\frac{\mathrm{d}^2q_1}{\pi}\cdots\frac{\mathrm{d}^2q_n}{\pi}\,\pi\,\delta^{(2)}(q_1 + \cdots + q_n - Q) \times\mathrm{e}^{-r_q^2(q_1^2+\cdots+q_n^2)}\,\frac{1}{n!} \sum_{n\ \text{connections}} F_P(Q_1, Q_2, Q_3)\,F_P(Q_1', Q_2', Q_3'), \quad t_n \simeq t/n. \tag{7}$$

The sum in this formula refers to all distinct ways to connect the beam and target quark lines with n Pomerons in the scattering diagram. The set of momenta Q_i and Q_l' the quarks acquire from the attached Pomerons is particular for each connection pattern. A more detailed description can be found in [5].

With the amplitude (4) the differential cross section in the normalization adopted here is evaluated as

$$\frac{\mathrm{d}\sigma}{\mathrm{d}t} \,=\, 4\pi\,|M_{pp}(s,t)|^2. \tag{8}$$

The optical theorem, which relates the total elastic cross section and the imaginary part of the amplitude, in this normalization reads

$$\sigma_{pp}^{\rm tot} = 8\pi \,{\rm Im}\, M_{pp}\ (s, t = 0).$$

Recall once more that exchanges of the positive signature Reggeons determine, strictly speaking, half of the sum of the pp and $p\bar{p}$ elastic amplitudes. Their difference is neglected in the present approach.

3 Cross section of single and double diffractive dissociation

Glauber theory makes it possible to find as well the cross sections of excitation or disintegration of one or both colliding objects. The close approximation (completeness condition) ([13,14] allows one to calculate the total cross sections of all processes related to the elastic scattering of the constituents but without giving rise to new particles production,

$$\frac{{\rm d}\sigma}{{\rm d}t}(pp \to p'p') = \frac{{\rm d}\sigma}{{\rm d}t}(pp \to pp) + 2\frac{{\rm d}\sigma}{{\rm d}t}(pp \to p^*p) + \frac{{\rm d}\sigma}{{\rm d}t}(pp \to p^*p^*).$$

Here ${\rm d}\sigma(pp \to pp)/{\rm d}t = {\rm d}\sigma_{\rm el}/{\rm d}t$ is the elastic pp scattering cross section shown in Fig. 2a. The situations when one scattered constituent receives a comparatively large transverse momentum is shown in Fig. 2b, c. In the case of nucleus–nucleus collisions it results in the excitation or disintegration of one of the nuclei. In the case of pp collisions in AQM a scattered quark moves far away from the remnant at the distance $\sim$1 fm, where a new $q\bar{q}$ pair is produced due to quark confinement effects. It can be interpreted as a diffractive production of single jets, $\sigma(pp \to pp^*) = \sigma_{\rm SD}$, say, of one or several pions, $p \to p + n \times \pi$. Similarly two diffractive jets are produced in the case of Fig 2d, $\sigma(pp \to p^*p^*) = \sigma_{\rm DD}$. In Fig 2e a new $q\bar{q}$ pair is produced as part of a multiperipheral ladder independently of the quarks wave function leaving it essentially intact. This process is related to the inelastic interaction of the constituents and does not contribute to ${\rm d}\sigma(p'p')/{\rm d}t$ in AQM.

The amplitude of single diffraction dissociation reads

$$M_{\rm SD}(s,t) = \int {\rm d}K\, {\rm d}K' \psi^*(k_i' + Q')\, \widetilde{\psi}_m^*(k_i + Q_i) \times V(Q, Q')\, \psi(k_i')\, \psi(k_i). \quad (9)$$

Here the wave function of one of the protons remains unchanged whereas the other proton turns into the p^* final state specified with the wave function $\widetilde{\psi}_m(k_i)$.

The double diffraction dissociation implies both protons to be in the p^* final states,

$$M_{\rm DD}(s,t) = \int {\rm d}K\, {\rm d}K' \widetilde{\psi}_m^*(k_i' + Q')\, \widetilde{\psi}_n^*(k_i + Q_i) \times V(Q, Q')\, \psi(k_i')\, \psi(k_i). \quad (10)$$

To obtain the cross section one has to square the modulus of the appropriate amplitude. Making no distinction between the individual final states it should be summed over m for the process of (9) or over m and n indices for the process of

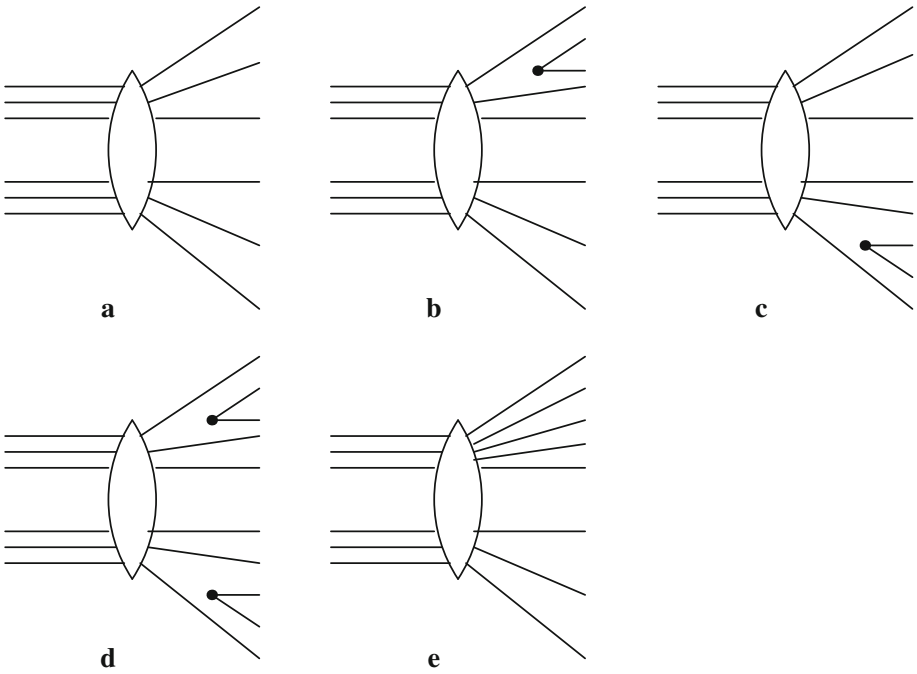

Fig. 2 Different final states in the high energy pp collision: **a** elastic pp scattering, **b** and **c** single diffractive dissociation of first or second proton, **d** double diffractive dissociation, **e** process with one $q\bar{q}$ pair inelastic production that does not contribute to the calculated $\sigma_{\rm SD}$ but can contribute to the experimental value $\sigma_{\rm SD}$

(10). For the DD case it gives

$$\frac{\mathrm{d}\sigma_{\rm el}}{\mathrm{d}t} + 2\frac{\mathrm{d}\sigma_{\rm SD}}{\mathrm{d}t} + \frac{\mathrm{d}\sigma_{\rm DD}}{\mathrm{d}t} = 4\pi \sum_{m,n} \int \mathrm{d}K\, \mathrm{d}K'\, \mathrm{d}P\, \mathrm{d}P'\, \widetilde{\psi}^*_m(k'_i + Q'_i)\, \widetilde{\psi}^*_m(k_i + Q_i) \times V(Q, Q')\psi(k'_i)\, \psi(k_i) \times \psi^*(p_i)\psi^*(p'_i)\; V^*(Q'', Q''') \times \widetilde{\psi}_m(p'_i + Q'''_i)\widetilde{\psi}_n(p_i + Q''_i). \quad (11)$$

Using now the completeness condition,

$$\sum_n \widetilde{\psi}_n(p_i + Q''_i)\, \widetilde{\psi}^*_n(k_i + Q_i) = \delta^{(2)}(p_i + Q''_i - k_i - Q_i)$$

along with the same condition for the index m we get

$$\frac{\mathrm{d}\sigma_{\rm el}}{\mathrm{d}t} + 2\frac{\mathrm{d}\sigma_{\rm SD}}{\mathrm{d}t} + \frac{\mathrm{d}\sigma_{\rm DD}}{\mathrm{d}t} = \int \mathrm{d}K\, \mathrm{d}K' \psi^*(k_i + Q_i - Q'''_i)\psi^*(k'_i + Q'_i - Q''_i) \times V(Q, Q')V^*(Q'', Q''')\psi(k'_i)\psi(k_i). \quad (12)$$

The double diffractive dissociation cross section is provided by the two sets of the Pomeron exchange diagrams separately associated with the "left" interaction vertex $V(Q, Q')$ and the "right" one $V^*(Q'', Q''')$. They are summed independently over the total numbers of the Pomerons participating in the diagram "from the left" or "from the right", $m, n = 1, 9$,

$$\frac{\mathrm{d}\sigma_{\rm el}}{\mathrm{d}t} + 2\frac{\mathrm{d}\sigma_{\rm SD}}{\mathrm{d}t} + \frac{\mathrm{d}\sigma_{\rm DD}}{\mathrm{d}t} = \sum_{m,n} |M^{(m,n)}_{p'p'}|^2(s, t).$$

Substituting here the Pomeron–quark vertex and the overlap function (6) introduced above, we express each term in the sum as

$$|M^{(m,n)}_{p'p'}|^2 = (\gamma_{qq}\mathrm{e}^{\Delta\cdot\xi})^{m+n}[\, i\eta_P(t_m)]^m\, [-i\eta^*_P(t_n)]^n \times \int \frac{\mathrm{d}^2q_1}{\pi} \cdots \frac{d^2q_m}{\pi}\, \pi\, \delta^{(2)}(q_1 + \cdots + q_m - Q) \times \frac{\mathrm{d}^2q_{m+1}}{\pi} \cdots \frac{d^2q_{m+n}}{\pi}\, \pi\, \delta^{(2)}(q_{m+1} + \cdots + q_{m+n} - Q) \times \mathrm{e}^{-r_q^2(q_1^2+\cdots+q_{m+n}^2)}\, \frac{1}{m!}\frac{1}{n!} \sum_{m,n \text{ connections}} \times F_P(Q_1, Q_2, Q_3)\, F_P(Q'_1, Q'_2, Q'_3). \quad (13)$$

For single diffractive dissociation the cross section includes the single sum over the final states of one of the protons. In this case the completeness condition gives

$$\frac{\mathrm{d}\sigma_{\rm SD}}{\mathrm{d}t} + \frac{\mathrm{d}\sigma_{\rm el}}{\mathrm{d}t} = 4\pi \sum_{m,n} |M^{(m,n)}_{pp'}|^2(s, t),$$

with

$$|M^{(m,n)}_{pp'}|^2 = (\gamma_{qq}\mathrm{e}^{\Delta\cdot\xi})^{m+n}[\, i\eta_P(t_m)]^m\, [-i\eta^*_P(t_n)]^n \times \int \frac{\mathrm{d}^2q_1}{\pi} \cdots \frac{\mathrm{d}^2q_m}{\pi}\, \pi\, \delta^{(2)}(q_1 + \cdots + q_m - Q) \times \frac{\mathrm{d}^2q_{m+1}}{\pi} \cdots \frac{\mathrm{d}^2q_{m+n}}{\pi}\, \pi\, \delta^{(2)}(q_{m+1} + \cdots + q_{m+n} - Q) \mathrm{e}^{-r_q^2(q_1^2+\cdots+q_{m+n}^2)} \times \frac{1}{m!}\frac{1}{n!} \sum_{m,n \text{ connections}} F_P(Q_1, Q_2, Q_3)\, F_P(Q'_1, Q'_2, Q'_3) \times F_P(Q''_1, Q''_2, Q''_3). \quad (14)$$

The first function F_P appears here from the completeness condition written for the dissociating proton, while the two other F_P functions in the product stand for an elastically scattered proton.

4 Numerical calculations

The expressions (13) and (14) have been used for the numerical calculation of the single and double diffractive dissociation of the protons together with Eq. (7) for their elastic scattering. The overlap function (6) is evaluated through the transverse part of the quarks' wave function, which has been taken in the simple form of two Gaussian packets,

$$\psi(k_1, k_2, k_3) = N[\, \mathrm{e}^{-a_1(k_1^2+k_2^2+k_3^2)} + C\, \mathrm{e}^{-a_2(k_1^2+k_2^2+k_3^2)}], \quad (15)$$

normalized to unity (2). One packet parametrization, $C = 0$, is insufficient to reproduce the experimental data on elastic scattering [5], imposing too strong a mutual dependence between the total cross section, the minimum position in $\mathrm{d}\sigma_{\rm el}/\mathrm{d}t$, and the value of the slope at $t = 0$. The two-exponential form of the quarks' wave function allows one to reproduce the exponential form for the summary differential cross section $\mathrm{d}\sigma_{\rm el}/\mathrm{d}t$, which is observed in LHC experimental data until the minimum region.

All parameters used in the calculation naturally fall into two different kinds: the parameters of the Pomeron and those specifying the structure of colliding particles. The former type, Δ, α', γ_{qq}, refers to the high energy scattering theory, while the latter, $a_{1,2}$ and C, details the matter distribution inside the proton in the low energy limit (similar to the density distribution in the atomic nuclear case).

We recalculate the elastic scattering cross section $\mathrm{d}\sigma_{\rm el}/\mathrm{d}t$, obtained in our previous paper [5] assuming the argument of the signature factor $t_n = t/n = -Q^2/n$, which is natural for a Gaussian Q^2 dependence. It causes a slight change of the model parameters. Now the Pomeron parameters are

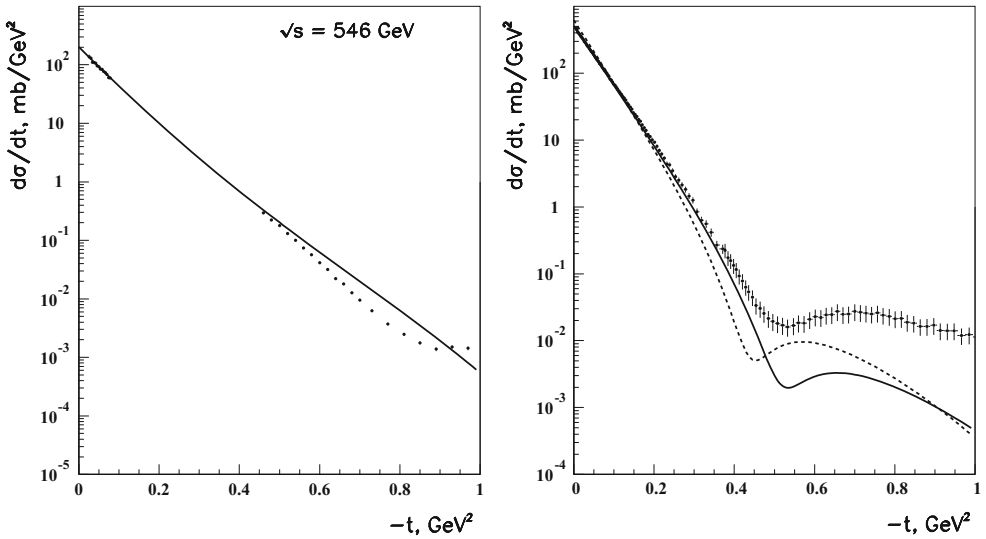

Fig. 3 The differential cross section of elastic $p\bar{p}$ scattering at $\sqrt{s} =$ 546 GeV (*left panel*) and for the elastic pp collisions at $\sqrt{s} = 7$ TeV (*right panel*, *solid line*) compared to the experimental data. The *dotted line* in the *right panel* shows the predicted elastic pp cross section at $\sqrt{s} = 13$ TeV. The experimental points have been taken from [15–18]

Table 1 The results obtained for the elastic, SD and DD cross sections

$\sqrt{s}$	$\sigma_{\rm el}$ (mb)	$\sigma_{\rm SD}$ (mb)	$\sigma_{\rm DD}$ (mb)
546 GeV	14.3	2.3	2.6
7 TeV	27.3	4.3	3.9
13 TeV	31.6	5.4	4.9

$$\Delta = 0.107, \quad \alpha' = 0.31\,\text{GeV}^{-2}, \quad \gamma_{qq} = 0.44\,\text{GeV}^{-2},$$

and the parameters of the matter distribution in the proton are

$$a_1 = 4.8\,\text{GeV}^{-2}, \quad a_2 = 1.02\,\text{GeV}^{-2}, \quad C = 0.133.$$

Note that the same set of the Pomeron parameters describes proton and antiproton scattering, therefore both pp and $p\bar{p}$ data have been commonly used to fix their values.

The model gives a reasonable description of elastic scattering experimental data both for pp collisions at $\sqrt{s} = 7$ TeV and $p\bar{p}$ collisions at $\sqrt{s} = 546$ GeV; see Fig. 3. The obtained curves are only slightly different from those published in the previous paper [5].

The results for the SD and DD cross sections are presented in Table 1. The SD cross sections turn out to be rather small, $\sigma_{\rm SD}/\sigma_{\rm el} \simeq$ 15–18 %, which probably matches the experimental results at LHC energies [19–21]. It might indicate that the contribution of the diagram in Fig. 2e is not large.

The total diffraction cross section is approximately half the elastic one, $2\sigma_{\rm SD} + \sigma_{\rm DD} \simeq \sigma_{\rm el}/2$, within the range of available energy dependence of the probability of diffractive to elastic scattering.

The ratio $\sigma_{\rm SD}/\sigma_{\rm el}$ is in somewhat inconsistency ($1.5 \div 2$ times smaller) with the intermediate energy estimation in [22]. We get $\sigma_{\rm SD} \approx \sigma_{\rm DD}$, so that $\sigma_{\rm DD}/\sigma_{\rm el}$ is not quadratically small compared to $\sigma_{\rm SD}/\sigma_{\rm el}$. The reason for this comes in AQM from an extra third form factor F_P in the SD cross section (14) compared to the two form factors in the DD formula (13). On the other hand, the connection between diffractive cross section calculated in AQM and the experimental data is not straightforward, since AQM comprises only a part of the processes involved in the scattering. The processes shown in Fig. 2e are not accounted for in AQM although their contribution to the experimentally measured $\sigma_{\rm SD}$ is quite possible.

Motivated by the recently announced new LHC run we present also the predictions for the elastic pp scattering and diffractive dissociation at $\sqrt{s} = 13$ TeV. In particular, we expect the total cross section $\sigma(pp)_{\rm tot} = 110$ mb, the parameter of the elastic slope cone ($\mathrm{d}\sigma/\mathrm{d}t \sim \exp(-B \cdot t)$) $B = 21.8\,\text{GeV}^{-2}$, the minimum position at $|t| = 0.45\,\text{GeV}^2$, while our results for the differential cross section, $\mathrm{d}\sigma_{\rm el}/\mathrm{d}t$, are shown in Fig. 3.

Figure 4 shows our results for the differential cross sections $\mathrm{d}\sigma_{\rm SD}/\mathrm{d}t$ and $\mathrm{d}\sigma_{\rm DD}/\mathrm{d}t$ at $\sqrt{s} = 546$ GeV. The slope of the differential cross section at $|t| \simeq 0.2$ GeV^2 is $B_{\rm SD} \simeq 10$ GeV^{-2} for the single diffractive diffraction and $B_{\rm DD} \simeq 3$ GeV^{-2} for the double diffractive dissociation. These values are essentially smaller than the elastic slope, which is about 15 GeV^{-2} [5].

Unfortunately we are unable to make predictions at small $|t| < 0.1$ Gev^2 because of the unknown effects of confinement, which could lead to the transition between the ground and excited states. However, such a transition cannot change

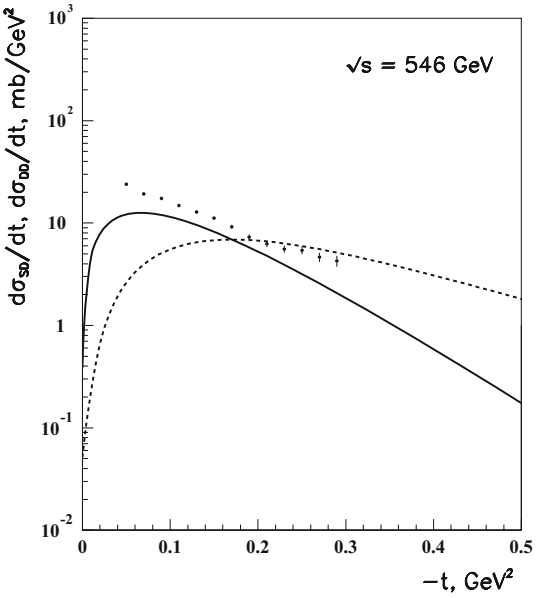

Fig. 4 The cross section of single (*solid line*) and double (*dotted line*) diffractive dissociation in $p\bar{p}$ scattering at $\sqrt{s} = 546$ GeV. The experimental SD points have been taken from [23]

the total cross sections (13), (14) calculated with the help of the close approximation. The region $|t| > 1$ Gev^2 is beyond the reach of our model as well, since the internal structure of the constituent quarks can no more be ignored there. The diffractive cross section behavior in the intermediate interval is in reasonable agreement with the experimental data.

5 Conclusion

We have presented the unified description of the elastic and diffractive pp ($p\bar{p}$) scattering in the framework of AQM. The main feature of our model is the common set of parameters it employs. After fitting the parameters that describe the elastic scattering no more ones have been added for the diffractive case. The parameters chosen are mainly determined by the structure of the quark wave function for the initial state.

The ratio r_q^2/r_p^2, which is responsible for AQM applicability, is not very small at the LHC energy ($r_q^2/r_p^2 \simeq 0.4$ at $\sqrt{s} = 7$ TeV [5]). Despite this the model yields reasonable predictions both for the elastic and diffractive dissociation pp scattering, qualitatively consistent with LHC experimental data in the region 0.1 Gev^2 $< |t| <$ 1 GeV^2.

Acknowledgments The authors are grateful to M.G. Ryskin for helpful discussion.

Funded by SCOAP[3].

References

1. I.M. Dremin, Phys. Usp. **56**, 3 (2013) (Usp. Fiz. Nauk., 183, 3, 2013). arXiv:1206.5474 [hep-ph]
2. M.G. Ryskin, A.D. Martin, V.A. Khoze, Eur. Phys. J. C **72**, 1937 (2012)
3. C. Merino, Y.M. Shabelski, JHEP **1205**, 013 (2012). arXiv:1204.0769 [hep-ph]
4. O.V. Selyugin, Eur. Phys. J. C **72**, 2073 (2012). arXiv:1201.4458 [hep-ph]
5. Y.M. Shabelski, A.G. Shuvaev, JHEP **1411**, 023 (2014). arXiv:1406.1421 [hep-ph]
6. E.M. Levin, L.L. Frankfurt, JETP Lett. **2**, 65 (1965)
7. J.J.J. Kokkedee, L. Van Hove, Nuovo Cim. **42**, 711 (1966)
8. Y.L. Dokshitzer, D. Diakonov, S.I. Troian, Phys. Rep. **58**, 269 (1980)
9. V.M. Shekhter, Yad. Fiz. **33**, 817 (1981) [Trans: Sov. J. Nucl. Phys. **33**, 426 (1981)]
10. V. N. Gribov, ZhETF **53**, 654 (1967) (Sov. Phys. JETP, 26, 414, 1968)
11. R. Avila, P. Gauron, B. Nicolescu, Eur. Phys. J. C **49**, 581 (2007). arXiv:hep-ph/0607089
12. R.J. Glauber, in *Lectures in Theoretical Physics*, eds. W.E. Brittin etal. (New York, 1959), vol. 1, p. 315
13. V. Franco, R.J. Glauber, Phys. Rev. **142**, 1195 (1966)
14. V.M. Braun, Y.M. Shabelski, Sov. J. Nucl. Phys. **35**, 731 (1982) (Yad. Fiz., 35, 1247, 1982)
15. F. Abe et al., CDF Collaboration, Phys. Rev. D **50**, 5518 (1994)
16. G. Antchev et al., TOTEM Collaboration, Europhys. Lett. **96**, 21002 (2011)
17. TOTEM Collaboration, G. Antchev et al., Europhys. Lett. **101**, 21002 (2013)
18. TOTEM Collaboration, G. Antchev et al., Europhys. Lett. **95**, 41001 (2011). arXiv:1110.1385
19. G. Antchev et al., TOTEM Collaboration, Europhys. Lett. **101**, 21003 (2013)
20. TOTEM Collaboration, F. Oljemark, K. Osterberg, Studies of soft single diffraction with TOTEM at $\sqrt{s} = 7$ TeV. LHC students poster session, 13 March 2013 (2013)
21. V.A. Khoze, A.D. Martin, M.G. Ryskin, Int. J. Mod. Phys. A **30**(08), 1542004 (2015). arXiv:1402.2778 [hep-ph]
22. A.B. Kaidalov, Phys. Rep. **50**, 157 (1979)
23. D. Bernard et al., UA4 Collaboration, Phys. Lett. B **186**, 227 (1987)